Using a MEMS gyroscope to stabilize the attitude of a fly-sized hovering robot

Sawyer B. Fuller[†], E. Farrell Helbling[†], Pakpong Chirarattananon, and Robert J. Wood[*]

ABSTRACT

Creating an autonomous flying vehicle the size of a honeybee presents a number of technical challenges because of its small scale. As vehicle wingspan diminishes, angular acceleration rates increase, necessitating sensing and control systems with high bandwidth. Hovering demonstrations have so far required feedback from high-speed motion capture cameras to estimate the angular velocity, attitude, and position of the vehicle to provide the continuous corrective feedback necessary to avoid tumbling. To achieve autonomous flight, it will be necessary to incorporate a suite of sensors carried onboard. Here we present a step in this direction by integrating a MEMS gyroscope onto an 80 mg flapping-wing micro air vehicle to provide attitude feedback in flight. This enables 2–5 s hovering flights in which the motion capture system provides only position feedback. Our vehicle, and likely others in the future of similar scale, is propelled by flapping wings that generate vibration. Our results indicate that the resulting accelerations, measured as high as 5 g by the sensor's accelerometer, significantly distort readings from the accelerometer but not the gyroscope.

1 INTRODUCTION

Significant challenges accompany the reduction of a flying robot to the size of a fly or bee. As vehicle size diminishes, conventional propulsion approaches (e.g. as in rotorcraft) become impractical because of physical scaling laws. For example, energy losses per unit mass of an electromagnetic motor increase as l^{-2} [1], where l is some characteristic length of the vehicle such as the chord length. Biological organisms at this scale instead use flapping wings [2]. Most small flying animals, from hummingbirds to flies, have evolved a convergent solution of hovering by flapping wings to overcome the low glide ratio of fixed wings at low Reynold's numbers [3]. The resulting unsteady aerodynamics augment lift [2, 4].
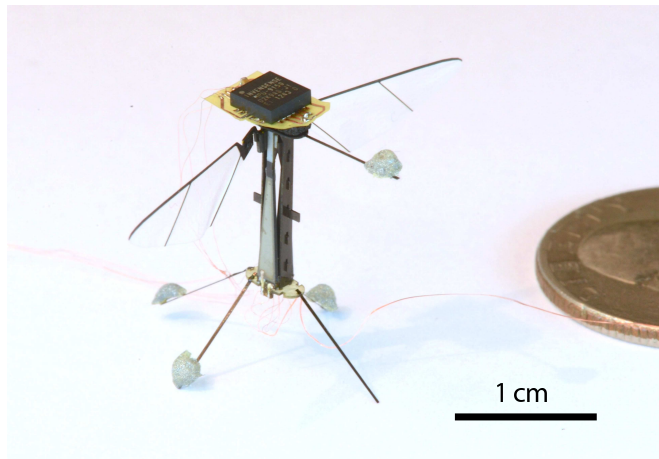

Figure 1: A robotic fly (81 mg) carries an onboard inertial measurement unit (40 mg) attached to the anterior to measure angular velocity. This feedback was used by the controller to apply corrective torques through the wings to stabilize its flight and hover.

The challenges at small scale extend to sensing and control. As the vehicle becomes smaller, the rate of rotational acceleration increases, scaling as l^{-1} [5]. This challenge is exacerbated by dynamic instability for designs that have the same basic body plan as hovering insects such as flies and bees, whose body hangs below the wings. Aeromechanics simulations suggest that typical baseline hovering wing kinematics lead to a dynamically unstable system [6, 7, 8]. Therefore, not only must a flight controller for such vehicles perform continuous corrective maneuvers as is required in fighter jets [9], it must do so with a time delay that is orders of magnitude shorter because of the smaller length scale. This is because fundamental control limits place an upper bound on the time delay that can be tolerated in a control loop that must stabilize a dynamically unstable system [10]. A vehicle the size of a fly or bee is nevertheless large enough that it is foreseeable that currently-available sensing and computation technologies could be miniaturized to fit within its mass and power constraints. An initial step toward flight autonomy is to equip a sensor that can stabilize its attitude dynamics.

The first fly-sized robot to carry its own weight overcame the propulsion challenge by driving flapping wings using piezoelectric actuators [4, 11]. Piezoelectric actuators have no moving components, allowing them to scale downward more favorably compared to motors that require

[*][†]Authors contributed equally. All authors are with the School of Engineering and Applied Sciences and the Wyss Institute for Biologically Inspired Engineering, Harvard University, Cambridge MA 02138 USA (E-mail: minster@seas.harvard.edu, ehelbling@seas.harvard.edu, pakpongc@seas.harvard.edu, and rjwood@eecs.harvard.edu)

bearings and gears [1]. A complementary laser-based microfabrication process was developed to quickly and precisely create flexure-based articulated mechanisms out of high-performance materials such as carbon fiber and polyimide [12].

Here we consider the attitude control problem of such a vehicle. Advances in fabrication and design led to an 81 mg prototype with the actuation capability to control its flight motions [13], shown in Figure 1. Using an array of external motion capture cameras and reflective markers attached to the vehicle to provide attitude and position feedback, a controller was developed that enabled it to perform controlled flight maneuvers [14]. To fly this vehicle autonomously outside of laboratory conditions, however, scale-appropriate sensing and control must be developed. Stability has previously been achieved with airfoils such as air dampers [7] or a tail [15, 16], but this makes the vehicle susceptible to wind disturbances and sacrifices maneuverability. An alternate approach, inspired by the ocelli of flying insects, achieved upright stability using four light-sensitive phototransistors and a light source above the vehicle [17]. In this work we use an inertial measurement unit (IMU) built from micro-electromechanical systems (MEMS) to provide information about the attitude of the vehicle so that it can stabilize its flight motions. Feedback from onboard gyroscopes has previously been used on flapping-wing vehicles, such as a 20 g hummingbird vehicle [18] and a 13 g four-winged ornithopter [15], but these vehicles are more than two orders of magnitude more massive.

Key questions to be addressed in the current study are whether the vehicle can be tuned to stably carry the weight of the sensor, which adds approximately 50% to the total vehicle weight, whether data can be returned through the tether with high fidelity, and whether the sensor's operation is disrupted by the high-frequency vibratory environment of flapping flight. In [18], it was found that certain MEMS gyroscopes produce nonsensical output when mounted on a flapping-wing vehicle. Gyroscope output was numerically integrated successfully to estimate absolute attitude for short periods on Baek's ornithopter [15]. Both of these platforms, however, flap at only ~20 Hz. It is therefore unknown whether sensor output will be disrupted at the much higher 120 Hz flapping frequency of our vehicle.

Our results show that by carefully calibrating the vehicle, it can carry the extra payload of the sensor. We find that neither communication nor gyroscopic fidelity is significantly disrupted by deployment on the tiny flapping-wing vehicle. In Sections 2 and 3, we describe the MEMS IMU and the flapping-wing micro air vehicle used in our test flights. In Section 4 we give an analysis of how rate feedback can give upright stability and demonstrate this principle using flight tests, reproducing earlier results using ocelli [17]. In Section 5 we show how this sensor was used to achieve short duration hovering, by demonstrating a series of flight tests

Table 1: Characteristics of the MPU9150 Inertial Measurement Unit

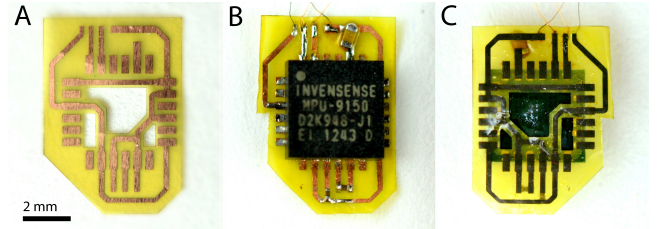| Characteristic	Typical Value
Mass	36 mg
Area	4×4 mm^2
Height	1 mm
Power	2.4 V, 9.4 mW
Max. Output Data Rate	
Gyroscope	8 kHz
Accelerometer	1 kHz
Magnetometer	8 Hz
Max. Range	
Gyroscope	$\pm 2000°$/s
Accelerometer	± 16g
Magnetometer	$\pm 1200 \mu$T
Max. Sensitivity	
Gyroscope	16.4 LSB/($°$/s)
Accelerometer	2048 LSB/g
Magnetometer	0.3 LSB/μT

Figure 2: IMU connected to the custom flex circuit. A) Unpopulated circuit board. B) Sensor and three capacitors (two 01-005 and one 04-02 size) after attachment to the circuit board, showing four-wire connection at the top. The outer border of the flex circuit has been modified from A to B to accommodate placement on the top of the robot. C) Populated circuit board shown from the back.

in which successively fewer components of external motion capture measurements are used for feedback control.

2 MEMS INERTIAL MEASUREMENT UNIT

2.1 Selection and Fabrication

The MPU9150 (Invensense, San Jose, CA, U.S.A.) was the first MEMS device to include a 3-axis accelerometer, a 3-axis gyroscope, and a 3-axis magnetometer in a package small enough for our robotic fly to carry (see Table 1 for specifications). It communicates using the I2C protocol, providing feedback rates as high as 1 kHz. This is a higher rate than the 500 Hz motion capture system which has previously been used to stabilize the robot [14]. The sensor requires a minimum of three capacitors—one bypass capacitor, a filter capacitor and a charge pump capacitor. In addition, the pins for external clock input, frame synchronization input, and the
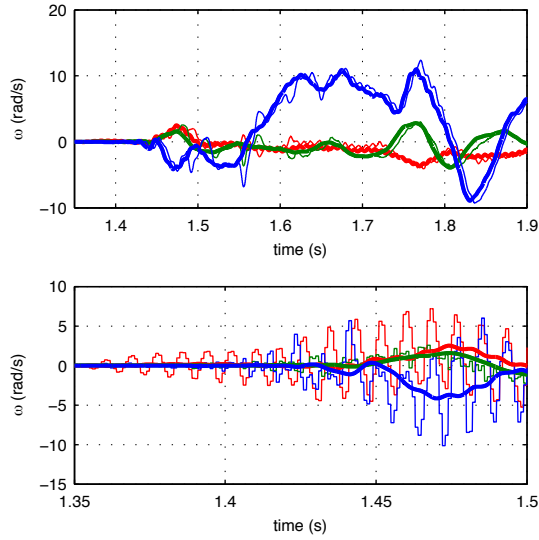
Figure 3: (top) Data from the flight in Figure 6 comparing filtered estimates of angular velocity ω from the gyroscope (thick lines) to that of the motion capture system (thin lines). The wings ramp-up flapping starting at t=1.35 s; red, green, and blue correspond to ω_x, ω_y, and ω_z, respectively. Spikes in the motion tracking estimates from the period t=1.5 to 1.7 s are due to imperfect tracking. (bottom) A close-up of readings from the gyroscope before filtering (thin lines, 1 kHz sampling frequency can be observed) and after filtering by a 3rd order low-pass Butterworth filter with a 40 Hz cutoff frequency. A prominent oscillation at the 120 Hz flapping frequency of the wings can be observed in the unfiltered measurements.

Figure 4: Accelerometer measurements in flight. (top) In a hovering test, the vehicle begins flapping its wings at t=2 s and flies to the setpoint altitude. (middle) A plot of accelerometer readings over a shorter time window shows the 120 Hz oscillations induced by the flapping wings and filtered version (approximately horizontal lines). Red, green, and blue are body x-, y-, and z-axis measurements, respectively. Accelerations up to ± 5 g are measured along the forward-backward direction of the flapping wings. (bottom) Motion capture estimate of acceleration (filtered, light line) compared to accelerometer measurements along the z-axis (filtered, dark line, data rotated to world frame).

slave address least significant bit need to be pulled low. The logic voltage and supply voltage were connected to reduce the number of wires and weight. To satisfy these requirements we designed a custom printed circuit board (flex circuit) to mount on the robot.

The sensor itself has a mass 36 mg (Table 1). The additional components of the capacitors, board, and solder added an additional 4 mg. In [13], measured lift forces indicated that the robotic fly could carry an additional 60-70 mg while flapping with a maximum wingbeat amplitude. But operating the wings at full amplitude leaves no capability to modulate wing kinematics to apply torques around the pitch and roll axes (Section 3). The lower the payload, the greater the control torques that can be applied. Accordingly, to minimize mass the board was made from thin copper-clad flex circuit material (18 μm copper, 12.7 μm polyimide). The circuit was fabricated using a direct-write photolithography and etching process and components were then hand-soldered (Figure 2). To minimize torque due to an off-axis placement, the sensor was attached at the anterior of the vehicle, as shown in Figure 1.
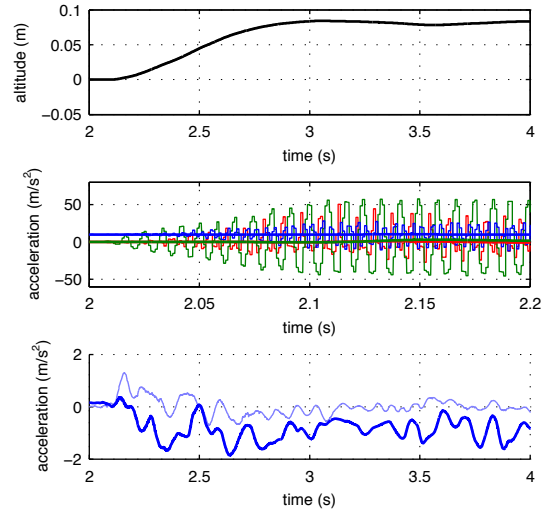
2.2 Communication interface and control

Sensor data was communicated over I2C at 400 kbps through four 51-gauge copper wires measuring approximately 30 cm. Control computations were performed by a desktop computer running an xPC Target realtime operating system (Mathworks, Natick, MA, USA). The data rate is sufficient to communicate gyroscope and accelerometer readings at a rate of 1 kHz. The control loop on this computer operated at 10 kHz to provide smooth analog signals to external high-voltage amplifiers. Because the I2C protocol requires digital communication at rates much higher than the control loop frequency, a field-programmable-gate-array (FPGA) add-in card (Speedgoat GmbH, Liebefeld, Switzerland) was programmed to implement the I2C protocol. A voltage level shifter (Phillips GTL2002) allowed digital electrical communication between the MPU9150 (max 3.3 V) and the FPGA board (5V TTL). Embedded Matlab software translated the 16-bit signed integer sensor readouts into floating point quantities for use in the controller.

2.3 Initial Characterization

To characterize the sensor, we compared the outputs of the gyroscope and the accelerometer to motion capture measurements during open and closed-loop flight experiments

(see Figure 3 (top) for comparison). The filtered gyroscope data reproduces the motion capture measurement faithfully, with approximately 10 ms less latency.

As can be seen in Figure 4, the measured acceleration along the z-axis of the robot can generally track the motion capture estimate; however, when the wings begin flapping at approximately t=2.1 s, the accelerometer estimate becomes negative (Figure 4). Given the altitude trajectory, we expect a positive acceleration at the start that approaches zero as the robot reaches the desired altitude. This is reflected in the motion capture measurement. The raw signal from the accelerometer, however, shows high frequency noise with a maximum amplitude of (± 5 g) along the y-axis. This is in the same direction as the forward-backward motion induced by the flapping wings. It is possible this large oscillation cross-couples to other degrees of freedom or moves the sensor into a nonlinear regime in which it is slightly less precise. The distortion is nearly -2 m/s^2, is larger than the accelerations of interest, which are on the order of 1 m/s^2 (Figure 4). Integrating this sensor's output twice to estimate position gives an error on the order of one meter within a second in all directions, suggesting it cannot be used for motion estimation except at very short timescales.

3 ROBOTIC FLY

As described in more detail in [13, 14], the robotic fly prototype considered here (Figure 1) has a pair of independently-actuated wings that can produce sufficient lift to take off and induce torques independently about orthogonal axes to control the vehicle's motion. We define a right-handed coordinate system for the body in which the right wing points along the positive x-axis, the y-axis points forward, and the z-axis points upward (Figure 5). In this definition, the long axis of the body hangs downward in the negative-z direction. Roll torque is induced by varying the relative stroke amplitudes of the left vs. right wing. Pitch torque is induced by moving the "mean stroke angle"–the time-averaged angle of the forward-backward motion of the wings–in front ($+y$) or behind ($-y$) the center of mass [13].

The robot is given power and controlled through a lightweight compliant tether wire that has little effect on vehicle dynamics [14, 17]. Power and control commands are transmitted over four 51-gauge (0.022 mm diameter) copper wires and feedback from the IMU is returned through a second bundle of four. Limitations in the current manufacturing process limit vehicle lifetime of each laboriously-fabricated vehicle [11] to just a few minutes of flight, after which flexure joints fail and the vehicle must be replaced. Accordingly, only a few flights were possible in this study.

4 UPRIGHT STABILITY IN FLIGHT

The simplest way to utilize a gyroscope to stabilize flight motions is to take advantage of the natural dynamics of the vehicle. In previous work [17] it was shown analytically and
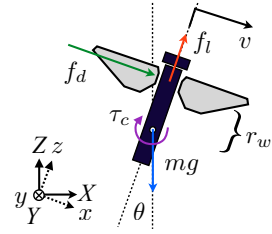

Figure 5: Model and axis convention for the robotic fly. The vehicle state is given by three quantities, the rotation angle θ, the rotation velocity ω, and the lateral velocity in body coordinates v. A lift force f_l generated by the flapping wings acts at a distance r_w away from the center of mass and along the body-z direction, an aerodynamic drag force f_d acts at a distance r_w from the CM, and the gravitational force mg acts at the center of mass. The right-handed axis convention for world coordinates is shown, with y pointing into the paper. A feedback controller applies a control torque τ_c by altering baseline wing kinematics.

experimentally on the flapping-wing robot testbed that stability of the vehicle can be achieved by applying a torque proportional to the angular velocity in the pitch and roll directions. This is because the body of the robotic fly hangs below the wings, exhibiting pendulum-like dynamics that are unstable without feedback, but can be stabilized through a velocity-proportional feedback that induces a "damping" effect. In that work, an ocelli-inspired light sensor was used to estimate angular velocity. Here, we first aimed to verify whether angular velocity feedback measured from the gyroscope could be used as a substitute.

4.1 Stability Analysis

A diagram of the planar dynamics is shown in Figure 5. A test of this vehicle flapping in a wind tunnel indicated that the stroke-averaged drag force on the wings is nearly linear with the incident airspeed for typical wing kinematics. This is the case for wind in both the x- and y-directions. Accordingly, the model for aerodynamic drag in both cases is:

$$f_d = -b_w v_w,$$

where v_w is the lateral velocity of the point on the airframe at the midpoint between the two wings and b_w is a drag constant. If the vehicle is rotating at angular velocity ω, then the velocity of the wings, when linearized around $\theta = 0$, is $v_w = r_w \omega + v$, where r_w is the distance from the midpoint of the wings to the CM. Similarly, the force arising from aerodynamic drag is $f_d = -b_w(v + r_w \omega)$ and the torque about the center of mass due to this force is $\tau_d = -r_w f_d = b_w r_w v - b_w r_w^2 \omega$. With lift force due to the flapping wings (f_l) approximately balancing out weight (mg), the lateral force due to the tilted thrust vector is equal to $-f_l \sin \theta = -mg \sin \theta \approx -mg\theta$ for small θ.

With a control law that applies a torque proportional to the rate of rotation,

$$\tau_c = -k_d\omega, \qquad (1)$$

and assuming planar motion, we can neglect second-order cross-product terms and equate forces and torques to velocities according to $f = m\dot{v}_x$ and $\tau = J\dot{\omega}$. The linearized equations of motion about zero pitch angle θ can be written as a state-space dynamical system $\dot{\boldsymbol{q}} = A\boldsymbol{q}$ with the state vector $\boldsymbol{q} = [\theta, \omega, v]^T$ expressed in body coordinates, where

$$A = \begin{bmatrix} 0 & 1 & 0 \\ 0 & -\frac{1}{J}(b_w r_w^2 + k_d) & \frac{1}{J}b_w r_w \\ -g & \frac{b_w r_w}{m} & -\frac{b_w}{m} \end{bmatrix}. \qquad (2)$$

Using the Routh-Hurwitz stability criterion gives a lower bound on the velocity feedback gain in the controller given in Equation (1) necessary to achieve asymptotic stability at $[\theta, \omega, v] = \mathbf{0}$ for the robotic fly. Using previously-published parameters and the addition of the 40 mg mass of sensor the on the anterior of the robot, 1.5 mm above the leading edge of the wing, we found that a gain of $k_d = 2 \times 10^{-7}$ was sufficient to achieve stability for both xz- and yz- dynamics.

4.2 Flight Tests

Tuning in preparation for closed-loop flights was initiated as follows. If the vehicle is sufficiently well-fabricated that it can take off without a torque bias, then the direction of pitch or roll velocity after take-off is observed. Trim values for pitch and roll torque are altered to the maximum extreme to oppose its initial torque. If in the subsequent take-off the vehicle is observed to apply a net torque in the opposite direction, the vehicle is deemed worthy of further testing. A search is then performed to find trim parameters for which takeoff is nearly vertical.

The vehicle's flight trajectory with feedback from the gyroscope alone is shown in Figure 6. In this flight, feedback from the gyroscope was applied according to the control law in Equation (1). The vehicle remains stably upright during this flight, indicating that gyroscopic feedback is able to stabilize its upright orientation as desired. Without feedback, in all trials yet observed, the vehicle quickly tumbles.

5 HOVERING

In this section we build on the demonstration of achieving upright stability using gyroscope feedback to demonstrate hovering using a combination of gyroscope feedback and motion capture.

The hovering controller used here incorporates improvements over that reported in [14] that includes an adaptive component that continuously estimates vehicle parameters such as torque offsets [19]. We provide an overview here. The flight controller requires three inputs: angular velocity $\boldsymbol{\omega}$ (body coordinates), attitude $[\hat{\boldsymbol{x}}, \hat{\boldsymbol{y}}, \hat{\boldsymbol{z}}] = R^T$ (the unit vectors of the axes of the vehicle in world coordinates, equivalent to the transpose of the rotation matrix R), and position
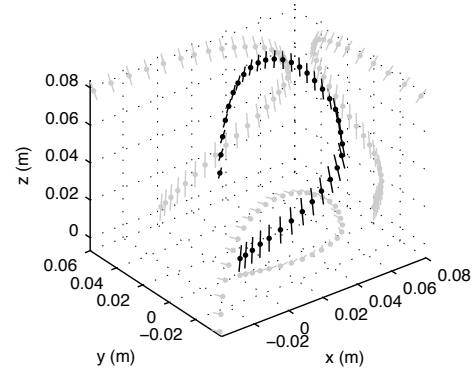

Figure 6: Plot of flight trajectory in which angular velocity feedback from the gyroscope was used to maintain an upright orientation. In this flight, position was not under feedback control. Vehicle attitude is rendered at 20 ms intervals. Dots represent the location of the CM of the vehicle and the black line denotes the long axis of the body; projections of the trajectory are shown in grey in the background. In the z-projection below the vehicle, the "forward" $+y$ direction of the vehicle is projected rather than its long axis to indicate the vehicle's heading.

$[X, Y, Z]^T$ (world coordinates). An independent altitude controller modulates the thrust force to maintain the desired altitude given position feedback. An outer position loop computes a desired direction of the $\hat{\boldsymbol{z}}$ vector, $\hat{\boldsymbol{z}}_d$, based on the position error. By inclining the axis of the vehicle, lateral thrusts can be generated. The attitude error is defined as $\boldsymbol{e} = [\hat{\boldsymbol{y}} \cdot \hat{\boldsymbol{z}}_d, -\hat{\boldsymbol{x}} \cdot \hat{\boldsymbol{z}}_d, 0]^T$. Based on this error, the attitude controller calculates torques as a function of the attitude error $\boldsymbol{e}$ and angular velocity $\boldsymbol{\omega}$ according to:

$$\begin{aligned} \tau_c &= f(\mathbf{e}, \omega) + \tau_o \\ &= -K_a(\omega + \Lambda\mathbf{e}) - (\Lambda\mathbf{e} \times \mathbf{J}\omega) - \mathbf{J}\Lambda\dot{\mathbf{e}} + \tau_o \quad (3) \end{aligned}$$

where K_a and Λ are positive diagonal gain matrices that are experimentally tuned, τ_o is the trimmed offset torque necessary to compensate for manufacturing irregularity, and $\mathbf{J}$ is the estimate of the inertia matrix.

To use gyroscope feedback in this controller, note that the output of the three-axis gyroscope is an estimate of $\boldsymbol{\omega}$. Additionally, from Equation (3), an estimate of attitude error $\boldsymbol{e}$ is needed. We parameterize the vehicle attitude using a zyx-convention for Euler Angles to avoid representation singularities at hover. In this convention, attitude is defined by first rotating the frame by an angle $\theta_3 \in (-\pi, \pi]$ (yaw) around the body z-axis, then $\theta_2 \in \left(-\frac{\pi}{2}, \frac{\pi}{2}\right)$ (roll) around the new body y-axis, and then $\theta_1 \in \left(-\frac{\pi}{2}, \frac{\pi}{2}\right)$ (pitch) around that body x-axis. Performing the same rotations about world axes but in the opposite order, that is, XYZ, gives the same attitude. With this convention, the rates of change of these angles as a function of the angular velocity vector $\boldsymbol{\omega}$ are given by the
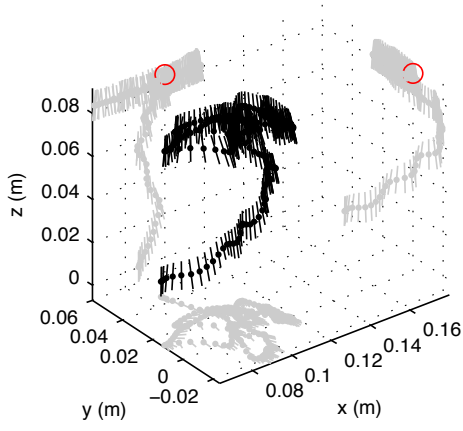
Figure 7: Plot of flight trajectory, rendered at 20 ms intervals. This flight used feedback entirely from motion capture, providing a baseline performance measure. The desired hovering position is indicated by a red circle. Other figure conventions are the same as in Figure 6.
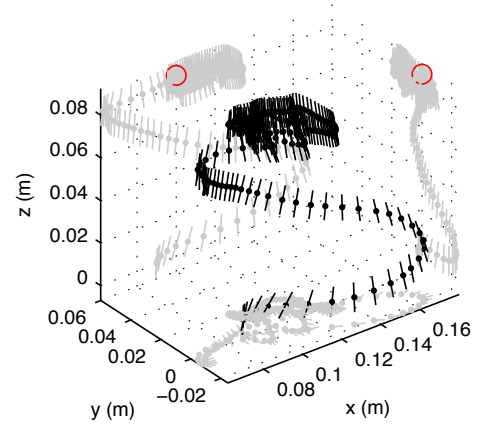

Figure 8: Plot of hovering flight trajectory in which gyroscope provided an estimate of the angular velocity $\boldsymbol{\omega}$. Other details are the same as in Figure (7).

product

$$
\begin{bmatrix} \dot{\theta}_1 \\ \dot{\theta}_2 \\ \dot{\theta}_3 \end{bmatrix} = \begin{bmatrix} \cos\theta_3/\cos\theta_2 & -\sin\theta_3/\cos\theta_2 & 0 \\ \sin\theta_3 & \cos\theta_3 & 0 \\ -\cos\theta_3\tan\theta_2 & \sin\theta_3\tan\theta_2 & 1 \end{bmatrix} \begin{bmatrix} \omega_1 \\ \omega_2 \\ \omega_3 \end{bmatrix}.
$$
(4)

By integrating Equation (4) over time, an estimate of the attitude can be computed from the rotation matrix derived from these Euler Angles [19], from which e and its derivative can be computed.

Because of the limited lifetime of the robot, we performed the experiments incrementally. First, we verified that hovering was operational using only feedback from motion capture, insuring that the necessary amount of control authority was available after incorporating the additional payload, and to quantify a baseline flight performance. Next, we incorporated the angular velocity estimate $\boldsymbol{\omega}$ from the gyroscope into the feedback loop. Finally we additionally incorporated the attitude estimate $\hat{z}$ derived from integrating gyroscope output (Equation (4)) so that motion capture feedback was entirely eliminated from attitude control of the robot.

5.1 Motion Capture Feedback

Figure 7 shows that, with appropriate tuning of controller gains and trim values, the robot was able to carry the extra payload and take off and hover near the desired setpoint position $[X, Y, Z]^T = [0.1, 0, 0.06]^T$ m using motion capture feedback. Its mean position for the 2 s period after reaching the desired altitude was $[0.109, 0.0077, 0.056]^T$ m.

5.2 Angular Velocity Feedback

Having demonstrated in Section 2 that the angular velocity estimate of $\boldsymbol{\omega}$ from the gyroscope accurately tracks the ground truth measurement from motion capture, with lower latency, we incorporated this estimate into the hovering attitude controller. Figure 8 shows that the robot achieves hovering flight, flying near the set point, maintaining a mean position of $[0.093, 0.0058, 0.056]^T$ m and comparable error.

5.3 Attitude Feedback

In this experiment, we performed a zero-order hold numerical integration of Equation (4), initialized using the motion capture estimate of attitude at $t=0$ s. Figure 9 shows the trajectory of the robot during a flight in which both angular velocity and attitude were estimated by feedback from the onboard gyroscope. In this experiment the robot remained near the setpoint position for approximately 2 s, after which it began to exhibit significant position error. This may be attributable to drift in the attitude estimate causing a lateral thrust error. During the initial 2 s period of tracking, the robot maintained a mean position of $[0.075, 0.029, 0.057]^T$ m.

5.4 Analysis

The flight using only motion capture estimates produced a mean Euclidean distance error of less than 0.01 m from the setpoint. When the $\boldsymbol{\omega}$ estimate from the gyroscope was incorporated, the mean error was a comparable 0.01 m. For the flight in which gyroscope feedback additionally estimated the attitude $\hat{z}$, the error increased to 0.03 m. A possible explanation for the error is that, as can be observed in Figure 10, a visible drift is noticeable along the pitch (red) axis, reaching an error of 6° (0.1 rad). This drift, perhaps arising because the largest oscillations occur about this axis because of the forward-backward motions of the wings (Figure 3), would cause a force error in the y-direction as the vehicle tilted in response.

In addition to plotting the 3D trajectory of each flight and comparing the mean position of each flight experiment, we calculated the root mean square error (RMSE, see Figure 11). We expect comparable levels of RMSE in altitude because
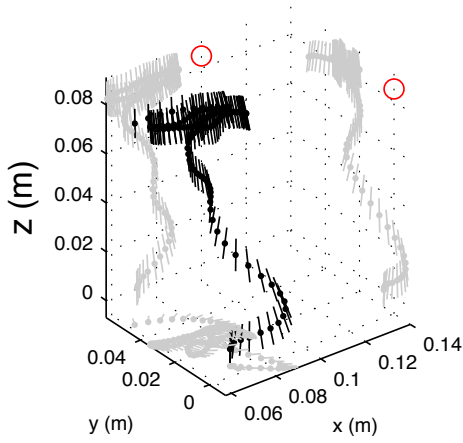
Figure 9: Plot of flight trajectory in which the gyroscope provided all attitude feedback in the flight controller, including both angular velocity ω and attitude $\hat{z}$. In this flight, the position error was somewhat larger than in Figure (8), possibly because of drift in the attitude estimate. Other details are the same as in Figure (7).

the altitude controller runs independently of the attitude controller and receives the same measurements in all tests, as can be observed in Figure 11. RMSE is comparable between the motion capture-only experiment and experiment in which the gyroscope estimated ω for both x-position, where the errors are 1.17 cm and 1.39 cm, respectively, as well as for the y-position, where the errors are 1.26 cm and 1.05 cm, respectively. The RMSE of the lateral position of the flight with attitude estimation from the gyroscope is significantly larger at 2.72 cm in $x-$position and 2.95 cm in y-position. Given that the robot had difficulty correcting its pitch angle and drifted away from the set point during flight, these values are not unexpected. These results indicate that estimates from the gyroscope can be substituted for those from the motion capture system and still maintain stability and control of the vehicle despite its fast and unstable dynamics.

6 CONCLUSIONS

In this work we demonstrated a MEMS IMU integrated with a fly-sized robotic vehicle. Feedback from this sensor was shown to be sufficient to stabilize this vehicle's upright orientation and estimate the vehicle's attitude for short periods for use in an inner attitude control loop. This constitutes the first demonstration of controlled flight in fly-sized robot in which only position feedback was derived from external sensors.

Our results indicate that gyroscope sensor readings are somewhat, though not significantly impaired by vibrations induced by the wings. Because the flapping frequency is known, a future improvement could refine the filter design to better eliminate it, either by a notch filter or by adaptive cancellation, and thus reduce feedback latency even further.
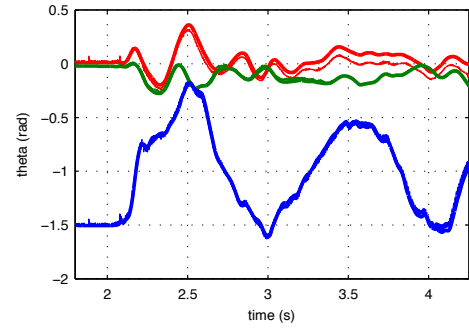

Figure 10: Comparison of measured Euler Angles – pitch (red), roll (green), and yaw (blue) – from motion capture (thin line) to the estimate derived by integrating gyroscope feedback (thick line) from the flight shown in Figure (9). The flight starts at t=2.0 s. Drifting over time can be observed, particularly about the x-axis (pitch).
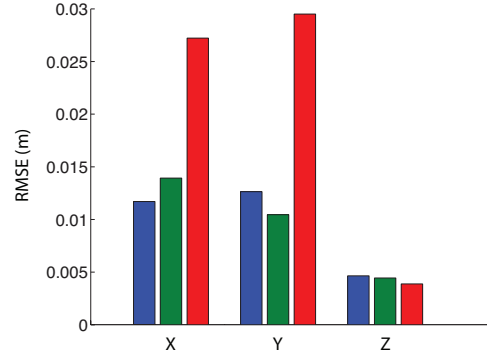

Figure 11: Root Mean Square Error (RMSE) position error for x-, y-, and z-coordinates for three flight experiments: motion capture feedback (blue), ω estimate from gyroscope (green), and full attitude measurements ($\omega, \hat{z}$) from gyroscope (red).

Our results indicate that the accelerometer component exhibited significant noise and distortion in the presence of the flapping wings. This suggests alternative sensing modes may be necessary to quickly sense translational motions for high-bandwidth control, such as infrared proximity sensors, vision, or a pressure sensor (for altitude). We cannot rule out that sonar or laser rangefinders could be sufficiently miniaturized.

As the fabrication process matures, more flights will be possible, which will permit a more comprehensive characterization of the system dynamics presented here. To permit longer flight times, drift in the attitude estimate could be reduced by incorporating accelerometer or magnetometer feedback using a Kalman Filter.

The results reported here provide a baseline sensor suite for stable flight that will enable future flight control studies. They motivate further development in lightweight sensing,

computation, power source, and control technologies appropriate for bee- or fly-sized flying vehicles.

7 Acknowledgements

References

[1] W. S. N. Trimmer. Microbots and micromechanical systems. *Sensors and Actuators*, 19:267–287, 1989.

[2] Robert Dudley. *The biomechanics of insect flight: form, function, evolution*. Princeton University Press, 2002.

[3] U. Pesavento and Z.J. Wang. Flapping wing flight can save aerodynamic power compared to steady flight. *Physical review letters*, 103(11):118102, 2009.

[4] R. J. Wood. The first takeoff of a biologically inspired at-scale robotic insect. *IEEE Transactions on Robotics*, 24(2):341–347, 2008.

[5] Vijay Kumar and Nathan Michael. Opportunities and challenges with autonomous micro aerial vehicles. *The International Journal of Robotics Research*, 31(11):1279–1291, 2012.

[6] Leif Ristroph, Gunnar Ristroph, Svetlana Morozova, Attila J. Bergou, Song Chang, John Guckenheimer, Z. Jane Wang, and Itai Cohen. Active and passive stabilization of body pitch in insect flight. *Journal of The Royal Society Interface*, 10(85), 2013.

[7] Zhi Ern Teoh, Sawyer B. Fuller, Pakpong C. Chirarattananon, Nestor O. Perez-Arancibia, Jack D. Greenberg, and Robert J. Wood. A hovering flapping-wing microrobot with altitude control and passive upright stability. In *Intelligent Robots and Systems (IROS), 2012 IEEE/RSJ International Conference on*, pages 3209–3216, Vilamoura, Algarve, Portugal, 7–12 October 2012. IEEE.

[8] Imraan Faruque and J. Sean Humbert. Dipteran insect flight dynamics. Part 1: Longitudinal motion about hover. *Journal of Theoretical Biology*, 264(2):538–552, 2010.

[9] Malcolm J. Abzug and Eugene E. Larrabee. *Airplane stability and control, Second Edition: A history of technologies that made aviation possible*. Cambridge University Press, Cambridge, MA, 2002.

[10] Karl Johan Astrom and Richard M. Murray. *Feedback Systems: An Introduction for Scientists and Engineers*. Princeton University Press, 41 William Street, Princeton, NJ 08540, 2008.

[11] Robert J. Wood, Ben Finio, Michael Karpelson, Kevin Ma, Nestor O. Pérez-Arancibia, Pratheev S. Sreetharan, Hiroto Tanaka, and John P. Whitney. Progress on "pico" air vehicles. *The International Journal of Robotics Research*, 31(11):1292–1302, 2012.

[12] JP Whitney, PS Sreetharan, KY Ma, and RJ Wood. Pop-up book mems. *Journal of Micromechanics and Microengineering*, 21(11), 2011.

[13] Kevin Y. Ma, Samuel M. Felton, and Robert J. Wood. Design, fabrication, and modeling of the split actuator microrobotic bee. In *Proceedings of the IEEE Int Robotics and Automation Conference*, pages 1133–1140, St. Paul, MN, 14–18 May 2012. IEEE.

[14] Kevin Y. Ma, Pakpong Chirarattananon, Sawyer B. Fuller, and Robert Wood. Controlled flight of a biologically inspired, insect-scale robot. *Science*, 340(6132):603–607, 2013.

[15] Stanley S Baek, Fernando L Garcia Bermudez, and Ronald S Fearing. Flight control for target seeking by 13 gram ornithopter. In *Intelligent Robots and Systems (IROS), 2011 IEEE/RSJ International Conference on*, pages 2674–2681. IEEE, 2011.

[16] C. De Wagter, S. Tijmons, B.D.W. Remes, and G.C.H.E. de Croon. Autonomous flight of a 20-gram flapping wing mav with a 4-gram onboard stereo vision system. In *Robotics and Autonomous and Systems (ICRA), 2014 IEEE/RSJ International Conference on*, Hong Kong, China, 2–5 June 2014. IEEE.

[17] Sawyer B. Fuller, Michael Karpelson, Andrea Censi, Kevin Y. Ma, and Robert J. Wood. Controlling free flight of a robotic fly using an onboard vision sensor inspired by insect ocelli. *Journal of The Royal Society Interface*, 11(97), August 2014.

[18] Matthew Keennon, Karl Klingebiel, Henry Won, and Alexander Andriukov. Development of the nano hummingbird: A tailless flapping wing micro air vehicle. In *AIAA Aerospace Sciences Meeting*, pages 1–24, Reston, VA, 9–12 January 2012. AIAA.

[19] Pakpong Chirarattananon, Kevin Y Ma, and Robert J Wood. Adaptive control of a millimeter-scale flapping-wing robot. *Bioinspiration & biomimetics*, 9(2):025004, 2014.